

Cite this: *Mater. Horiz.*, 2018, 5, 708Received 12th March 2018,
Accepted 18th May 2018

DOI: 10.1039/c8mh00296g

rsc.li/materials-horizons

Fully 2D and 3D printed anisotropic mechanoluminescent objects and their application for energy harvesting in the dark†

Dinesh K. Patel,  Bat-El Cohen, Lioz Etgar  and Shlomo Magdassi *

We report on new material compositions enabling fully printed mechanoluminescent 3D devices by using a one-step direct write 3D printing technology. The ink is composed of PDMS, transition metal ion-doped ZnS particles, and a platinum curing retarder that enables a long open time for the printing process. 3D printed mechanoluminescent multi-material objects with complex structures were fabricated, in which light emission results from stretching or wind blowing. The multi-material printing yielded anisotropic light emission upon compression from different directions, enabling its use as a directional strain and pressure sensor. The mechanoluminescent light emission peak was tailored to match that of a perovskite material, and therefore, enabled the direct conversion of wind power in the dark into electricity, by linking the printed device to perovskite-based solar cells.

The biggest challenge in 3D printing is to integrate both form and function into the printed object. To overcome this challenge, one needs new functional materials and printing platforms. Among the 3D printing technologies available, direct ink writing (DIW) is a low-cost, high-speed process, based on layer-by-layer dispensing of a viscous liquid, capable of creating complex 3D structures in one step.^{1,2} To fabricate structures with good precision and composition, the ink used in DIW should fulfill two criteria: first, the rheological properties of the ink must be tailored so it flows through the dispensing nozzle and facilitates dispensing yet quickly retains the pre-designed shape of the deposited layer(s). Second, it must contain a high proportion of the functional building material, to minimize drying-induced shrinkage after printing.¹ DIW can be utilized for multi-material printing by using several print heads, thus enabling multiple functionalities when forming devices.³ DIW has been used in myriad applications such as bioelectronics,³

Conceptual insights

Mechanoluminescent (ML) materials have been reported for applications such as flexible sensors, dynamic mapping of personal signatures and generating light using wind energy. These devices were fabricated by using conventional processes such as casting, molding, and cutting, which limit the devices to simple shapes only, with mainly the utilization of one light emitting material, and a time consuming fabrication process. We present a new process and material composition to fabricate devices with complex structures and multimaterials. The process is based on the 3D printing of ML materials embedded within elastomeric monomers, by using a direct ink write (DIW) technology. The printing composition contained a curing retardant agent that enabled a long open time of the ink, thus overcoming the premature curing and blockage of the printing nozzle. Multimaterial printing enabled the patterning of ML objects with multiple color emissions that can be used in generating anisotropic light emission, which act as a directional sensor. In addition, we printed wind-driven ML devices, in one step, and coupling them with solar cells led to the direct conversion of wind energy into electricity in the dark. By using perovskite based solar cells, tailoring the absorbing material in the cell to the specific light emission of the ML device, enabled power generation higher than reported previously. We expect that these findings will lead to new ML-based applications such as embedded directional sensors, security inks and energy devices.

microfluidics,⁴ sensors,⁵ wave guides,^{6,7} catalyst carriers,⁸ data storage,⁹ tissue engineering,¹⁰ graphene aerogels,¹¹ and drug-delivery systems.¹²

Mechanoluminescence was first demonstrated by Francis Bacon in 1605 by breaking sugar crystals.^{13,14} During the last few decades, researchers have devoted much attention to developing mechanoluminescent (ML) materials. The main studied ML materials are quartz,¹⁵ rocks,¹⁶ alkali halides,^{17,18} molecular crystals,¹⁹ rare earth ion-doped aluminates and silicates^{20,21} and zinc sulphide (ZnS).²² Rare earth ion-doped aluminates and silicates, along with ZnS display intense and repeatable mechanoluminescence. ZnS doped with transition metal ions (Cu⁺, Mn²⁺, and others) has been well studied for the fabrication of ML devices owing to the intense and durable mechanoluminescence.^{23–25} Intense, reproducible, and non-destructible ML can be obtained by combining transition metal ion-doped

Casali Center for Applied Chemistry, Institute of Chemistry, The Center for Nanoscience and Nanotechnology, The Hebrew University of Jerusalem, Jerusalem 9190401, Israel. E-mail: magdassi@mail.huji.ac.il

† Electronic supplementary information (ESI) available. See DOI: 10.1039/c8mh00296g

ZnS particles and stress transmission materials.²⁶ The most common stress transmission materials (transparent elastomeric matrix) are epoxy resins²⁷ and poly dimethyl siloxane (PDMS).^{23,26} High transparency, low cost, inertness, robustness, and high durability make PDMS an ideal candidate for a stress transmission material for fabricating ML devices with high brightness.^{22,26} Devices containing PDMS and ZnS were studied for both their fundamental and technological applications,²³ while being fabricated by using conventional processes such as casting, molding, and cutting,^{23,24,26} which limit the devices to simple shapes only, by using mainly commercially available materials.^{23–26} ML devices have found applications in the fields of flexible sensors,^{28,29} dynamic mapping of personal handwriting/signatures,³⁰ generating light using wind energy,²³ structural health monitoring (SHM) for composite materials/polymers,³¹ artificial skin,³² and piezophototronic luminescence devices.³³ 3D printing of ML devices with complex geometries in one step will not only save time and fabrication cost, but also open a window for a wide variety of new applications based on unique geometries and multi-wavelength emission for directional ML and energy harvesting in the dark.

Here, we report for the first time on fully 2D and 3D printed ML devices using DIW material printing. The ML devices consist of ZnS doped with transition metal ions, PDMS, and a platinum curing retarder that enables a sufficient open time (Fig. S1a, ESI†) for performing the printing process. Fig. 1a schematically presents the printing process for ML devices. It consists of an extruder loaded with viscous ink; it is externally cooled using an ice and salt mixture. Fig. 1b shows a 3D printed ML candy structure, and the inset shows a photograph of emitted green light under UV illumination (365 nm). Fig. 1c shows the generated ML spectrum and Fig. 1d shows a photograph of the object under compression and release (see mechanoluminescence in Movie S1, ESI†). Fig. 1e(i–iv) shows fully printed ML objects having various geometries. These structures show

green luminescence under UV exposure at 365 nm (Fig. S2, ESI†) and green mechanoluminescence upon compression and release (Fig. 1f). DIW even enables the fabrication of 3D printed cube shaped balloons (Fig. S3a, ESI†), which show green luminescence upon blowing with compressed air, with a peak centered at 515 nm (Fig. S3b and Movie S2, ESI†).

The printed objects were tested for their ability to produce light by wind blowing. In the past, wind-driven ML devices were fabricated using multiple steps, *i.e.*, casting on a mold followed by cutting.²³ Similar compositions of inks with various doping levels of ZnS were printed with the aim of obtaining ML devices for light harvesting. Fig. 2a demonstrates fully printed wind-driven ML objects having different light emission spectra. The thicknesses of these wind driven ML devices were about 700–800 μm . The setup used to generate light by wind (here by nitrogen gas, where the flow rate is controlled by the gas cylinder pressure) is shown in Fig. 2b. The dependence of the ML intensity and spectra on gas flow for various doping levels of the ZnS particles is shown in Fig. 2c–e (green, orange and blue) and Movie S3 (ESI†). As presented, for all objects, an increase in the flow rate led to an increase in the emitted light intensity, whereas the positions of the emission peaks were almost unchanged (515 and 586 nm, respectively), except for the blue-emitting object for which we observed a blue shift (Fig. S4, ESI†). Fig. 2d shows the CIE plot of the emitted light. For a blue wind-driven ML device, a significant shift in the CIE coordinates (0.20, 0.53 to 0.18, 0.42) was observed, but for a green-emitting ML device, a minimal shift was observed. For an orange wind-driven ML device, there was no shift in the CIE coordinates (Fig. 2f).^{23,24}

With the knowledge of the CIE plots, we aimed to prepare white ML light by combining orange- and blue-emitting phosphors. Fig. 3(a–c) shows the emission spectra obtained from printed wind-driven ML objects containing different weight ratios of orange and blue phosphors, *i.e.*, 7:3, 5:5, and 3:7.

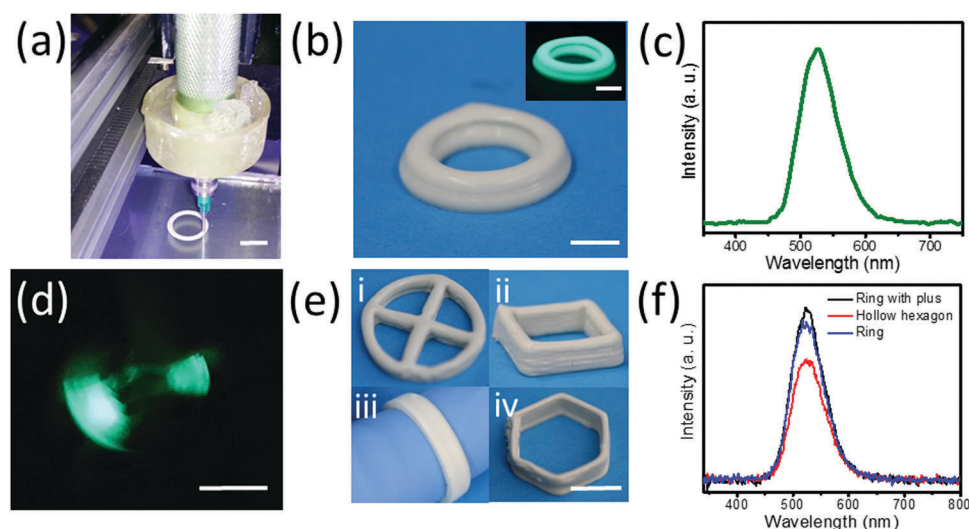


Fig. 1 (a) Printing of a ML device (in process), (b) 3D printed ML candy (the inset shows a photograph of green light-emitting candy under UV exposure), (c) a luminescence spectrum generated from the ML candy, (d) a photograph of the ML candy under compression and release, and (e) a ring with a plus at the center, a hollow square, a ring, and a hollow hexagon (i–iv), and (f) their ML spectra under continuous stretching and release. The scale bar is 10 mm.

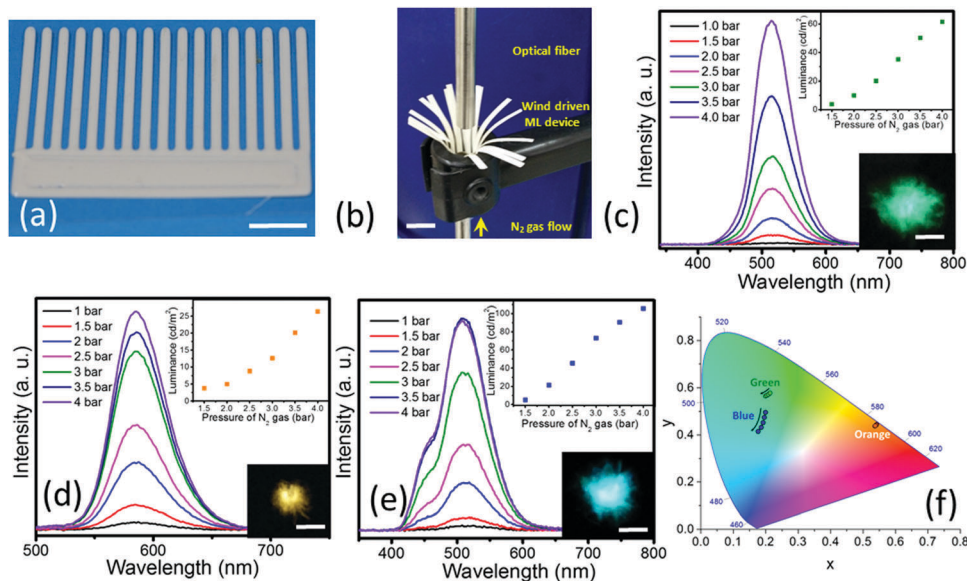


Fig. 2 (a) A fully printed wind-driven ML device; (b) a setup for measuring ML from a printed wind-driven device; (c–e) ML spectra of wind-driven green (c), orange (d), and blue (e) devices (the upper insets show the luminance with varying pressures of nitrogen gas flow, and the lower insets show photographs of the corresponding ML devices) and (f) CIE coordinates from the wind-driven green, orange, and blue ML devices. The scale bar is 10 mm.

The upper inset shows the dependence of luminance intensity on the gas flow rate and the lower inset shows a photograph taken from the wind-driven objects. The luminance observed in our study from the orange and blue phosphors with a 3:7 ratio was around 132 cd m^{-2} (Movie S4, ESI[†]), which is much higher than previous reports on ML for generating white light (50 cd m^{-2} and 21 cd m^{-2}).^{23,33} Jeong *et al.* have used orange and blue phosphors in a 7:3 ratio,²³ whereas Chen *et al.* have used a commercial white phosphor with unknown composition

for the generation of white light.³³ Fig. 3d shows the CIE diagrams of these devices with different weight ratios of orange and blue-emitting ZnS. It was observed that an increase in the weight ratio of the blue phosphor results in a systematic shift from orange to white light. These results are in agreement with previous reports.²³ As seen in Fig. S5 (ESI[†]), we could generate cool white light using a weight ratio of orange:blue ZnS (7:3) with a correlated color temperature (CCT) of 3861 K; the CIE coordinates lie on black body radiation (Planckian locus). Wind driven ML devices have been demonstrated earlier for light harvesting, including white light generation, but were fabricated with conventional and time consuming processes, moulding and cutting.^{23,26} By the proposed process, we overcome these drawbacks and provide a simple additive manufacturing process with tailored material composition.

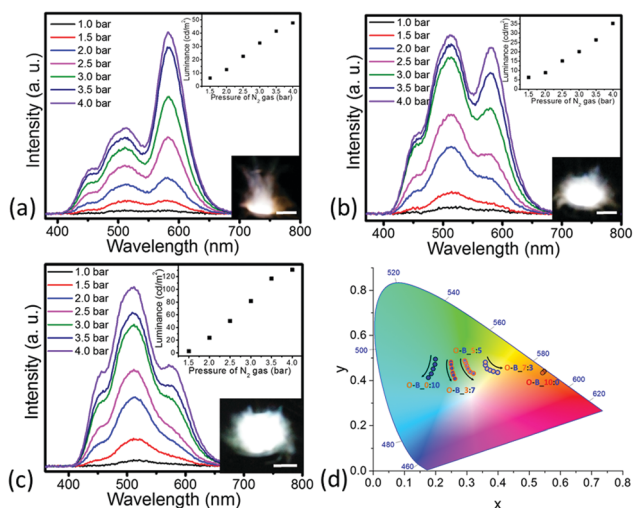


Fig. 3 Fully printed wind-driven ML devices with different ratios of orange- and blue-emitting ZnS in the PDMS matrix; ratio: (a) 7:3, (b) 5:5, and (c) 3:7 (the insets show the luminance under varying pressures of nitrogen gas flow and the lower insets show the photographs of luminescence from the devices) and (d) CIE coordinates from wind-driven ML for different ratios of orange (O) to blue (B) from 0:10 to 10:0. The scale bar is 10 mm.

Such printed wind-driven ML devices were further evaluated for energy harvesting. Solar energy harvesting can be performed only at daytime by using solar cells or thermosolar devices. If the solar cells can also function at night, this will be a significant advantage. We suggest performing energy harvesting using solar cells in the dark, while the solar cells are illuminated with light generated by wind-driven ML devices. The schematic representation of energy harvesting in the dark using a perovskite solar cell linked to a wind-driven ML device is shown in Fig. 4a. The main requirement for this approach is to match the ML spectra to the absorption spectra of the perovskite. Indeed, the absorbance of the perovskite layer is shown in Fig. 4b; the layer has a strong absorbance ($n = \infty$) at around 520 nm, whereas the green wind-driven ML device exhibits emission maxima at around 515 nm. Thus, absorbance from the perovskite and green ML emission overlaps well; and hence, it can be used for energy harvesting. In this setup, the solar cell was placed above the wind-driven ML devices and it

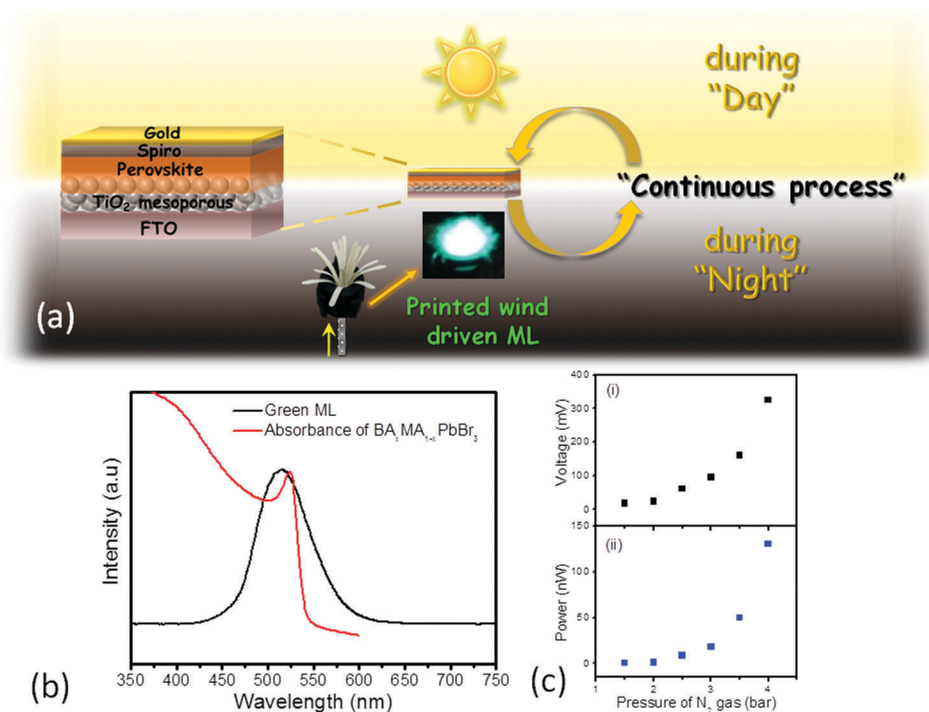


Fig. 4 (a) Schematic representation of energy harvesting in the dark using a wind-driven ML device and a perovskite-based solar cell, (b) absorbance of a perovskite-based solar cell and ML emission from a wind-driven ML device with a green phosphor, and (c) voltage and power generated by a wind-driven ML device coupled with a perovskite-based solar cell.

was illuminated by light obtained from ML generated by nitrogen flow, at varying pressures. The output voltages and power generated are shown in Fig. 4c. It was observed that, with an increase in the pressure of nitrogen gas, the voltage and power generated increase. We also carried out the same experiment with a wind-driven ML device using orange and blue phosphors in a 5:5 ratio for energy harvesting in the dark (Fig. S6b, ESI†). We observed that the voltage and current generated from this device are lower compared with the green-emitting device (Fig. S6b, ESI†) since the luminance (Fig. 3b, upper inset) is lower compared with that of the green ML devices (Fig. 2c, upper inset). Terasaki *et al.* have demonstrated energy harvesting from a ML device using a SrAl₂O₄:Eu pellet and a single crystal silicon based solar cell. ML was generated by applying different loads on the SrAl₂O₄:Eu pellet and the process was destructive.³⁴ In our report, we used wind driven ML for energy harvesting in the dark, by combing a printed ML object with a perovskite based solar cell and its absorption can be tuned. The power generated in this process is higher than previously reported, but at this point it is lower than that obtained during the day time. Therefore, future efforts will be directed towards increasing the light emission output.

Utilizing 3D printing technologies enables the structuring of ML objects composed of multimaterials that are localized in functional shapes. Fig. S7a and d (ESI†) present fully printed patterned green/orange ML square and hexagonal meshes (thickness around 1 mm) that emit light upon stretching (Fig. S7c and Movie S5, ESI†), which were printed within 10 minutes. For a comparison, Jeong *et al.* have demonstrated the fabrication of

multicolor-patterned devices using a complex multiple step process; the time required for the fabrication of the device was around 5 days.³⁵ This device could emit a light pattern only if both an electric field and stretching are applied.³⁵

DIW technology enables the printing of objects composed of multi-materials in a simple one-step process, as presented in Fig. 5 for a hexagonal ML mesh having dual emission capability. The ML spectra generated from these meshes (by stretching and release), along with a photograph showing the green and orange light, are shown in Fig. 5b and c (Video S6, ESI†). We also printed concentric squares with an inner region that emits orange and an outer region that emits green (Fig. 5d). The thickness of this device was 3 mm. Fig. 5d(ii) shows the patterned image under excitation at 365 nm and Fig. 5e shows a photograph of a concentric square during compression and release. Fig. 5f shows ML spectra of a fully printed concentric square upon compression and release. ML spectra were recorded at three different regions (A, B, and C) as seen in Fig. 5e. 'A' corresponds to the interface between the two regions, yielding both green and orange emission (the intensity of orange emission at 586 nm is higher than that at 515 nm), 'B' corresponds to the center region and has only orange emission (586 nm), and 'C' corresponds to the outer region having mainly green emission (Fig. 5f). It should be emphasized that the objects with dual ML emission are fabricated in one printing process, without assembling parts, which is required by a conventional fabrication process. Furthermore, the dual emission enables a directional/anisotropic response, as shown in Fig. 6. We fabricated an 'anisotropic' mechanoluminescent (AML) device showing different ML light patterns while compressed

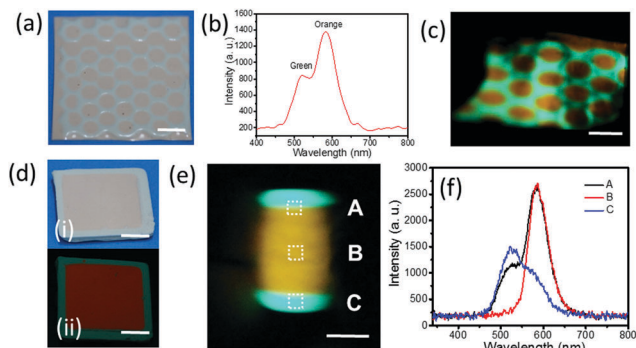


Fig. 5 Dual light-emitting patterned ML devices: (a) photograph of a patterned hexagonal mesh, (b) ML from the hexagonal mesh emitting green and orange, (c) a photograph of the hexagonal mesh under stretching and release, (d) a concentric square (i) without and (ii) under UV illumination (365 nm), (e) a ML image and (f) a ML spectrum at three regions: A, B, and C. The scale bar is 10 mm.

in different directions. When the AML device is compressed and released from the sides, *i.e.*, horizontally, we observed two green patterns on the opposite sides and orange light at the center. Similarly, when an AML device is compressed from the opposite corners, *i.e.*, diagonally, we observed four green patterns on all sides (except the corners) and orange light at the center (Movie S7, ESI[†]). Clough *et al.* reported tensile anisotropy using mechanoluminescent dioxetane and an elastomer, but the emission was not visible to the naked eye, and different magnitudes of strain must be applied to obtain the signal, which was recorded by a sophisticated instrument/camera.³⁶

Conclusions

In summary, we reported fully printed ML devices of various geometries using the DIW technique. The wind-driven ML devices were printed in one step for the first time, and cool white light having a CCT of 3861 K and 48 cd m⁻² luminance was obtained from objects consisting of orange and blue phosphors. In this report, we have demonstrated a proof of concept for a small device for the direct conversion of wind power to electricity by linking it to perovskite-based solar cells. At present, the power generated is low and efforts are needed to improve the performance in large scale operation. This can be

achieved by increasing the ML intensity through the use of multiple ML devices in parallel, or searching for materials which have higher ML intensity. Future efforts will be directed in this direction. We also demonstrated patterned ML devices that can emit single or dual colors. An anisotropic light ML emission was obtained upon compression from different directions, enabling their use as directional strain sensors. We expect that these findings will lead to new mechanoluminescence-based applications such as embedded sensors, security inks, and energy devices.

Experimental

Ink formulation for printing ML structures

To fabricate colored 2D and 3D printed ML structures, ML phosphor materials were mixed in PDMS. The PDMS base (Elastosil RT 601 A, Wacker) and cross-linker (Elastosil RT 601 B, Wacker) were weighed in a 9 : 1 ratio along with 1% by weight of platinum silicone cure retarder (SLO-JO, Smooth-On, Inc.) with respect to PDMS, which were mixed in a Thinky mixer for 2 min. The required amounts of ML material (Green GGS 42, Orange GG13, and Blue GGS 62, Mobichem Scientific Engineering, Ltd) were added to PDMS and stirred manually with the help of a glass rod. The ML material : PDMS weight ratio was maintained at 7 : 3. The mechanical properties of these compositions are evaluated and discussed in Fig. S1 (ESI[†]).

3D printing

ML devices were printed by System 30M (Hyrel 3D, USA), using a metallic extruder coupled with a nozzle with a size of 1.02 mm (18G). The thickness of each printed layer is around 500 μm. The build platform temperature was maintained at 40–50 °C. All ML structures were printed with a PDMS : phosphor ratio of 3 : 7 along with 1% curing retarder. The extruder was externally cooled by an ice-salt mixture, as presented in Fig. 1a, to further increase the open time of the ink. The use of the curing retarder and the external cooling ($T = 0-5$ °C) enabled an open time for a printing time of at least 30 minutes. The extrusion of the ink was controlled using Gcode with the REPETREL software provided by Hyrel Systems.

Perovskite cell fabrication

Perovskite precursor synthesis: methyl ammonium bromide (MABr) and benzylammonium bromide (BABr) were synthesized

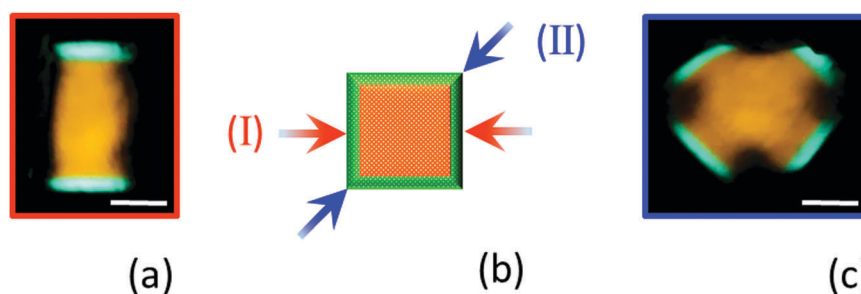


Fig. 6 Anisotropic mechanoluminescent (AML) device: photograph of an AML device on (a) horizontal compression and release from the sides (I, shown by red arrows), (b) schematic representation of an AML device, and (c) diagonal compression and release (II, shown by blue arrows). The scale bar is 10 mm.

for the fabrication of cells, as reported earlier and were used as precursors for the fabrication of perovskite-based cells.³⁷

Cell fabrication

A SnO₂:F (FTO) conductive glass (15 Ω cm⁻¹, Pilkington) substrate was coated by a TiO₂ compact layer (5000 rpm 30 s) prepared from a precursor solution of titanium diisopropoxide bis(acetylacetonate) (Sigma) in anhydrous ethanol (0.2 : 1 (v : v)) and was annealed at 450 °C for 30 min. The TiO₂ nanoparticle paste (20 nm, dyesol) was diluted to a 1 : 4 ratio in ethanol absolute (Sigma) and spin-coated (5000 rpm, 30 s) onto the substrate and annealed at 500 °C for 30 min. The substrate was then treated with TiCl₄ (70 °C, 30 min) and annealed again at 450 °C for 30 min. The perovskite layer was deposited on the substrate by two-step spin coating (10 s 1000 rpm + 60 s 5000 rpm) from a precursor solution containing BABr (0.08 mM), MABr (2 M), and PbBr₂ (2.05 M) in γ-butyrolactone/dimethylsulphoxide (1 : 1 (v : v)). During the second spin coating, 40 μL of toluene was added dropwise on the perovskite layer. After the perovskite was deposited, the films were annealed at 110 °C for 1 hour. The hole transporting layer was deposited onto the substrates by the spin coating of a 40 μL solution at 4000 rpm for 30 s after an initial 30 s of loading time. The HTM solution contains 0.072 g of 2,2',7,7'-tetrakis-(N,N-di-4-methoxyphenylamino)-9,9'-spirofluorinein, 1 mL of chlorobenzene with additives of 17.5 μL/1 mL bis(trifluoromethane)sulfonimide lithium salt in acetonitrile (520 mg mL⁻¹), and 28.8 μL/1 mL of 4-*tert*-butylpyridine (Aldrich). A ~70 nm-thick gold electrode was thermally evaporated on the film under a vacuum of ~10⁻⁷ Torr. Perovskite and hole transporting layer depositions were carried out in a nitrogen-filled glove box.

Energy harvesting in the dark

A perovskite cell was connected to a voltage/current-measuring device and was placed above a wind-driven ML device, as seen in Fig. 4a. Varying pressures of N₂ gas were passed through a wind-driven ML device and the output was measured using a voltmeter (EX310 multi-meter, Extech instruments) and a Keithley 2400 source meter (a Tektronix company).

Characterization

ML spectra were recorded using a fiber-coupled StellarNet BLUE-Wave spectrometer. All ML spectra were recorded with a 2 s integration time and 0.5 nm resolution in the range of 340 to 1100 nm at room temperature. The CIE coordinates and CCT were calculated from the ML spectra. Illuminance was measured using a Digital Lux Meter, Dr Meter, LX1330B, China, and was converted into brightness/luminance as reported.³⁸ The photos and videos were recorded using a Canon EOS 1200D camera equipped with a Tamron SP Di macro lens. The rheologies of the inks were measured using a Rheo Stress 6000 Rheometer (Thermo Scientific) and the mechanical properties of the resins (Fig. S1, ESI[†]) were evaluated using a Universal Testing Machine (INSTRON 3345, 500 N load cell) as reported earlier.³⁹

Conflicts of interest

There are no conflicts to declare.

Acknowledgements

This research was partially supported by the Singapore National Research Foundation, Prime Minister's Office, Singapore, under the CREATE program: Nanomaterials for Energy and Water Management, and by the Israel National Nanotechnology Initiative FTA project on functional coatings and printing.

References

- 1 J. A. Lewis, *Adv. Funct. Mater.*, 2006, **16**, 2193–2204.
- 2 J. A. Lewis, J. E. Smay, J. Stuecker and J. Cesarano, *J. Am. Ceram. Soc.*, 2006, **89**, 3599–3609.
- 3 A. E. Jakus, E. B. Secor, A. L. Rutz, S. W. Jordan, M. C. Hersam and R. N. Shah, *ACS Nano*, 2015, **9**, 4636.
- 4 J. Moorthy, G. A. Mensing, D. Kim, S. Mohanty, D. T. Eddington, W. H. Tepp, E. A. Johnson and D. J. Beebe, *Electrophoresis*, 2004, **25**, 1705–1713.
- 5 J. H. Holtz and S. A. Asher, *Nature*, 1997, **389**, 829–832.
- 6 D. N. Christodoulides, F. Lederer and Y. Silberberg, *Nature*, 2003, **424**, 817–823.
- 7 S. T. Parker, P. Domachuk, J. Amsden, J. Bressner, J. A. Lewis, D. L. Kaplan and F. G. Omenetto, *Adv. Mater.*, 2009, **21**, 2411–2415.
- 8 G. S. Chai, I. S. Shin and J. S. Yu, *Adv. Mater.*, 2004, **16**, 2057–2061.
- 9 D. A. Parthenopoulo and P. M. Rentzepis, *Science*, 1989, **245**, 843–845.
- 10 J. Y. Kim and D.-W. Cho, *Microelectron. Eng.*, 2009, **86**, 1447–1450.
- 11 C. Zhu, T. Y.-J. Han, E. B. Duoss, A. M. Golobic, J. D. Kuntz, C. M. Spadaccini and M. A. Worsley, *Nat. Commun.*, 2015, **6**, 6962.
- 12 Y. Y. Li, F. Cunin, J. R. Link, T. Gao, R. E. Betts, S. H. Reiver, V. Chin, S. N. Bhatia and M. J. Sailor, *Science*, 2003, **299**, 2045–2047.
- 13 F. Bacon, *Novum Organum (1620)*, PF Collier & Son, New York, 1902, p. 45.
- 14 F. Bacon, *Advancement of Learning and Novum Organum*, Colonial Press, 1900, vol. 18.
- 15 G. N. Chapman and A. J. Walton, *J. Appl. Phys.*, 1983, **54**, 5961–5965.
- 16 Y. Enomoto and H. Hashimoto, *Nature*, 1990, **346**, 641–643.
- 17 A. J. Walton, *Adv. Phys.*, 1977, **26**, 887–948.
- 18 B. P. Chandra, A. K. Bagri and V. K. Chandra, *J. Lumin.*, 2010, **130**, 309–314.
- 19 B. P. Chandra and J. I. Zink, *J. Chem. Phys.*, 1980, **73**, 5933–5941.
- 20 M. Akiyama, C.-N. Xu, Y. Liu, K. Nonaka and T. Watanabe, *J. Lumin.*, 2002, **97**, 13–18.
- 21 N. Terasaki, H. Zhang, H. Yamada and C.-N. Xu, *Chem. Commun.*, 2011, **47**, 8034–8036.
- 22 V. K. Chandra, B. P. Chandra and P. Jha, *Appl. Phys. Lett.*, 2013, **103**, 161113.

- 23 S. M. Jeong, S. Song, K.-I. Joo, J. Kim, S.-H. Hwang, J. Jeong and H. Kim, *Energy Environ. Sci.*, 2014, **7**, 3338–3346.
- 24 S. M. Jeong, S. Song and H. Kim, *Nano Energy*, 2016, **21**, 154–161.
- 25 S. W. Shin, J. P. Oh, C. W. Hong, E. M. Kim, J. J. Woo, G.-S. Heo and J. H. Kim, *ACS Appl. Mater. Interfaces*, 2016, **8**, 1098–1103.
- 26 (a) S. M. Jeong, S. Song, S.-K. Lee and B. Choi, *Appl. Phys. Lett.*, 2013, **102**, 051110; (b) S. M. Jeong, S. Song, S.-K. Lee and N. Y. Ha, *Adv. Mater.*, 2016, **25**, 6194–6200.
- 27 X. Chao-Nan, Z. Xu-Guang, A. Morito, N. Kazuhiro and W. Tadahiko, *Appl. Phys. Lett.*, 2000, **76**, 179–181.
- 28 N. Terasaki and C. N. Xu, *IEEE Sens. J.*, 2013, **13**, 3999–4004.
- 29 Y. Gun Jin, R. Mohammad Reza, G. Amir Hossein, L. Gong-Cheol and C. Jun-Seong, *Smart Mater. Struct.*, 2013, **22**, 055006.
- 30 X. Wang, H. Zhang, R. Yu, L. Dong, D. Peng, A. Zhang, Y. Zhang, H. Liu, C. Pan and Z. L. Wang, *Adv. Mater.*, 2015, **27**, 2324–2331.
- 31 K. Srivatsava, W. Hugo Van der, V. Vijay and S. Vishnu Baba, *J. Intell. Mater. Syst. Struct.*, 2017, **28**, 2458–2464.
- 32 C. N. Xu, T. Watanabe, M. Akiyama and X. G. Zheng, *Appl. Phys. Lett.*, 1999, **74**, 1236–1238.
- 33 L. Chen, M.-C. Wong, G. Bai, W. Jie and J. Hao, *Nano Energy*, 2015, **14**, 372–381.
- 34 N. Terasaki, C.-N. Xu, Y. Imai and H. Yaamada, *Jpn. J. Appl. Phys.*, 2007, **46**, 2385–2388.
- 35 S. M. Jeong, S. Song, H. Kim, K.-I. Joo and H. Takezoe, *Adv. Funct. Mater.*, 2016, **26**, 4848–4858.
- 36 J. M. Clough, C. Creton, S. L. Craig and R. P. Sijbesma, *Adv. Funct. Mater.*, 2016, **26**, 9063–9074.
- 37 B.-E. Cohen, M. Wierzbowska and L. Etgar, *Sustainable Energy Fuels*, 2017, **1**, 1935–1943.
- 38 E. F. Schubert, *Light-Emitting Diodes*, Cambridge Univ. Press, Cambridge, UK, 2006.
- 39 D. K. Patel, A. H. Sakhaei, M. Layani, B. Zhang, Q. Ge and S. Magdassi, *Adv. Mater.*, 2017, **29**, 1606000.